CrystEngComm

Accepted Manuscript

ROYAL SOCIETY OF CHEMISTRY

www.rsc.org/crystengcomm

N-H···π induced configurational isomerism and the role of temperature in the *Z* to *E* isomerization of 2-fluoro-*N*′-(3-fluorophenyl) benzimidamide

Dhananjay Dey[a] and Deepak Chopra*[a]

[a]Crystallography and Crystal Chemistry Laboratory, Department of Chemistry, Indian Institute of Science Education and Research Bhopal, Indore By-Pass Road, Bhauri, Bhopal-462066, Madya Pradesh, India. Fax: +91-755-6692392

ABSTRACT

We have investigated the role of N-H···π interaction in the formation of *Z*/*E* configurational isomers (including dimorphism in the *E* isomer) of 2-fluoro-*N*′-(3-fluorophenyl)benzimidamide. The lowering of the crystallization temperature by ~20 °C results in a new form (*Z* isomer). Single crystal X-ray diffraction, thermal characterization (differential scanning calorimetry, hot stage microscope), FTIR spectroscopy and theoretical calculations have been used to validate the existence of different conformers in the solid state. The single point energy difference between the *E* and *Z* isomer is 21.8 kJ/mol and the energy barrier for the isomerization is 103.7 kJ/mole obtained from the theoretical calculations. The difference in thermal energy is similar to the results obtained from theoretical studies; signifying the role of temperature in polymorphism as well as in *Z/E* isomerization. A comprehensive analysis of the crystal packing and the energetic features have been performed based on the molecular conformation and supramolecular packing involving strong N-H···N hydrogen bond and weak C-H···N, C-H···F, C-H···N, N-H···π, C-H···π intermolecular interactions and π-π stacking to evaluate the role of intermolecular interactions in the solid state. Lattice energies have been calculated using PIXEL method. Hirshfeld surface fingerprint plots also provide a platform for the evaluation of the contribution of different atom···atom contacts which contribute towards the packing.

INTRODUCTION

Polymorphism [1] (ability to exist in different crystalline forms that have different arrangement of the molecules in the solid state) is very important not only in industry but also in different areas in solid state chemistry [2]. The molecules having several donor and acceptor groups are able to form multiple intermolecular interactions, especially through the existence of strong hydrogen bonding [3]. These interactions control the association of the

molecules, leading to the formation of supramolecular architectures and are of extreme significance in the area of crystal engineering [4]. Organic compounds containing structural fragments C=N, N-H can exhibit *E*/*Z* isomerisation [5]. These functions are the building blocks in supramolecular structures, chemo- and biosensors, molecular memory storage, molecular electronics and also useful in biological, pharmaceutical industry [6]. Experimental and theoretical studies reveal that the thermal isomerization process in imines occurs either by rotational or inversion mechanism [7]. It has been observed that the energy barrier arround the C=N double bond for *N*-aryl imines is less than 96.6 kJ/mol [8]. In 1991, configurational isomerization of benzophenone anils has been reported by Matthews *et al*. [9]. They have shown the interconversion of the stereoisomers with *Z* and *E* configuration. This was due to the rapid rearrangement of *E* to *Z* imine in an equilibrium mixture in solution. Just because of the change in temperature (ambient temperature to 0ºC) from an ethanol solution, the *E* isomer changed to the *Z* isomer in the crystal. Benzamidines and their derivatives have a lot of applications in the synthesis of heterocyclic compounds [10]. Aromatic and hetero-aromatic imines particularly containing strong electron withdrawing groups in the *para* position of the phenyl ring can undergo *E*/*Z* isomerisation around the C=N double bond [11]. Furthermore, several *N*-arylbenzamidines have interesting biological properties, including inhibitor activity towards tyrosine kinases [12] and nitric oxide synthetase [13] and as selective D_1 dopamine receptor antagonists [14]. Antimicrobial [15] and antiparasitic [16] activities have also been reported [17]. The presence of the fluorine atom in the molecule is responsible for major changes in the physico-chemical properties, the chemical reactivity and the biological activity rather than the non-fluorinated analogues [18]. Organic fluorine has been observed to behave differently in an organic environment and its contribution in the context of crystal engineering is now widely established [19].

N-H···π interaction [20] was first reported in 1959 by Oki and Imamura from the IR spectra of *N*-benzylaniline and its derivatives [21]. In 1989, Motohiro Nishio has proposed that N-H···π interaction is an attractive force occurring between a hard acid (N-H) and a soft base (π-system) [22]. Seiji Tsuzuki and their co-workers have shown that the intermolecular interaction energy of N-H···π calculated from the extrapolated MP2 interaction energy at the basis set limit and a CCSD (T) correction term is 9.4 kJ/mol [23]. Rao et al. have studied the role of N-H···π interaction in the structural stability on a set of 100 different trans-membrane proteins and their results suggests that the N-H···π interactions contribute significantly to the overall stability and folding of trans-membrane proteins [24].

Keeping in mind the importance of N-H···π interaction; we have synthesized a series of fluoro derivatives of phenylbenzimidamide. In the current study, we have observed N-H···π induced polymorphism of the *E*-isomer (**E1** and **E2**) along with the *Z*-isomer (**Z**) of 2-fluoro-N-(3-fluorophenyl)benzimidamide and we have shown the role of temperature in the *Z* to *E* isomerization during the heating of the ***Z*** isomer.

EXPERIMENTAL SECTION

Synthesis

In a 10.0 ml round bottom flask (containing stirrer bar), 0.69 gm of powdered anhydrous aluminium chloride (1.2 eq^{v}.) was taken with 0.47 ml of 2-fluorobenzonitrile (1 eq^{v}.) at room temperature (25ºC) on an oil bath. A guard tube (filled up with anhydrous calcium carbonate) was attached on top of the flask. Then the mixture was heated up to 100ºC until a homogeneous melt (aluminium chloride.2-fluorobenzonitrile complex) was formed. To this 0.41 ml (1eqv.) of 3-fluoroaniline was added at a time. The whole mixture was heated at 120ºC and stirred for 6 hours. Then it was allowed to cool down to room temperature. The resultant solid was crushed and extracted with 20 ml aqueous NaOH (12%) solution and 20 ml dichloromethane (2-3 times) into a separating funnel. Then the organic layer was washed with water and dried with Na_2SO_4. The final product (yield: 76%) was purified by silica gel chromatography (**Scheme 1**) and characterized by ^{1}H-NMR spectroscopy (**Figure S1**).

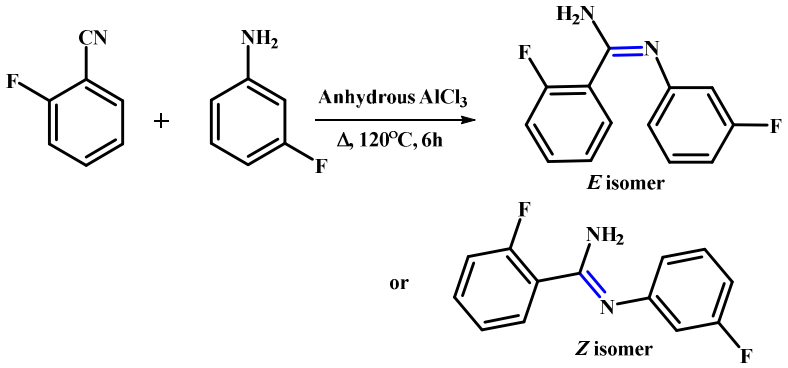

Scheme 1

Crystal growth and single-crystal X-ray Diffraction

Suitable single crystals for X-ray diffraction measurements were obtained through a solvent evaporation method. Synthesized compound was dissolved in polar/non-polar solvent and then kept at different conditions (varying the temperature). HPLC grade solvents were used

for the process of crystallization. Single-crystal X-ray measurements were carried out on a Bruker D8 venture PHOTON 100 CMOS diffractometer using monochromated MoKα radiation (λ = 0.71073 Å) in phi (φ) and omega (ω) scan at 100(2) K. The unit cell measurement, data collection, integration, scaling and absorption corrections for all these forms were performed using Bruker Apex II software [25]. The data collection was carried out giving an exposure time of 10 seconds per frame and a detector-to-crystal distance of 40 mm. The intensity data were processed by using the Bruker SAINT [26] suite of program. The crystal structures were solved by direct methods using SIR 92 [27] and refined by the full matrix least squares method using SHELXL97 [28] present in the program suite WinGX [29]. Empirical absorption correction was applied using SADABS [30]. The non-hydrogen atoms are refined anisotropically and the hydrogen atoms bonded to C and N atom, were positioned geometrically and refined using a riding model with $U_{iso}(H) = 1.2U_{eq}$ (C, N). The molecular connectivity was drawn using ORTEP32 [31] and the crystal packing diagrams were generated using Mercury 3.1 (CCDC) program [32]. Geometrical calculations were done using PARST [33] and PLATON [34]. The details of the data collection and the crystal structure refinement are shown in **Table 1**.

Crystallographic Modelling of Disorder

The occupancy of disordered fluorine (connected with the carbon atom either in *para* or *meta* position of the phenyl ring) at two positions was refined by using the PART command in SHELXL97, namely F1A & F1B and F2A & F2B ('A' contains the higher occupancy for that atom). The major part (A) contains around 90% occupancy for the fluorine atom and the minor part contains 10% occupancy for the fluorine atom. The anisotropic displacement parameter for these two sites is fixed using the EADP instruction.

Thermal characterization (Differential Scanning Calorimeter and Hot Stage Microscopy)

The melting points of these three forms including that of the bulk powder were measured with a Perkin-Elmer DSC 6000 instrument under nitrogen gas atmosphere. Accurately weighted samples (3-4 mg) were prepared in a covered aluminium pan and then allowed for the experiment with respect to a vacuum covered aluminium pan. The sample was heated from 30ºC to 110ºC with heating rate of 3ºC/min and again cooled to 30ºC. A total of two heating cooling cycles were performed. For hot stage microscopy (HSM) analysis, a stereomicroscope equipped with a hot stage apparatus was used. Photographs were taken by

Leica EC3 camera connected with the microscope. Single crystal of a particular form was placed on a glass slide and focussed under a microscope and then heated at 0.5ºC/min.

Table 1: Single Crystal Data Collection and Refinement.

Sample code	**E1**	**E2**	**Z**
Formula	$C_{13}H_{10}N_2F_2$	$C_{13}H_{10}N_2F_2$	$C_{13}H_{10}N_2F_2$
Formula weight	232.23	232.23	232.23
Temperature/K	100(2)	100(2)	100(2)
Wavelength (Å)	0.71073	0.71073	0.71073
Solvent system	Hexane, RT	Hexane, RT	DCM+ Hexane (4:1), LT
CCDC number	1016404	982079	1016405
Crystal system	Monoclinic	Monoclinic	Monoclinic
Space group	$P2_1/c$	$C2/c$	$P2_1/n$
a (Å)	12.7028(17)	23.4570(13)	6.7821(4)
b (Å)	8.3775(8)	11.7906(6)	22.9709(13)
c (Å)	11.5509(12)	8.1237(5)	6.9552(4)
α (˚)	90	90	90
β (˚)	117.017(5)	102.585(4)	91.464(4)
γ (˚)	90	90	90
V(Å^3)	1095.1(2)	2192.8(2)	1083.20(11)
Z	4	8	4
Density(g cm^{-3})	1.409	1.407	1.424
μ (mm^{-1})	0.109	0.109	0.110
F (000)	480	960	480
θ (min, max)	3.03, 30.07	1.78, 27.49	3.43, 30.41
Treatement of hydrogens	Fixed	Fixed	Fixed
$h_{min, max}$, $k_{min, max}$, $l_{min, max}$	(-17, 17), (-11, 11), (-16, 16)	(-30, 22), (-15, 12), (-10, 10)	(-8, 9), (-29, 30), (-9, 9)
No. of ref.	29721	9243	10701
No. of unique ref./ obs. Ref.	3065, 2378	2515, 1445	2672, 2173
No. parameters	162	162	162
R_{all}, R_{obs}	0.0685, 0.0503	0.1049, 0.0555	0.0541, 0.0431
$wR2_{all}$, $wR2_{obs}$	0.1379, 0.1263	0.1547, 0.1305	0.1113, 0.1044
$\Delta\rho_{min, max}$ (eÅ^{-3})	-0.429, 0.383	-0.306, 0.326	-0.357, 0.313
G. O. F.	1.026	1.040	1.053

Theoretical calculation

All the theoretical calculations have been performed considering the major conformation of the molecule only. The relative stabilities of the 2-fluoro-*N*′-(3-fluorophenyl)benzimidamide isomers were investigated using DFT calculations and the geometrical optimization of the isolated molecule was performed using DFT-B3LYP/6-31G** in TURBOMOLE [35] taking the crystal geometry as a starting model. Single point energies were calculated at DFT B3LYP/6-31G** level. In order to evaluate the energies associated with various non-covalent interactions present in the crystal, PIXEL calculations have been performed. The total lattice energy of the molecule is divided into the corresponding Coulombic, polarization, dispersion and repulsion energies [36]. Furthermore, the interaction energies obtained from the PIXEL module were compared with the values achieved from DFT+Disp calculation using B97-D/

aug-cc-pVTZ in TURBOMOLE. To get more insights into the molecular conformation about *E/Z* isomerization, we have carried out the conformational analysis using DFT-B3LYP/6-31G**. The AIMALL calculations for some selected dimers at the crystal geometry (with the hydrogen atoms moved to their neutral value) were performed at the DFT-B3LYP/6-311++G** level using Gaussian 09. The formatted checkpoint file (fchk) was used as an input file for AIMALL (version 13.05.06) [37] calculation. The electron density features at the bond critical points, which are computed, is as follows: (i) electron density (ρ_b), (ii) Laplacian ($\nabla^2\rho_b$) and (iii) kinetic energy density (G_b). E_{int}= 0.429 G_b (in au) [38]. The vibrational frequency analysis of the N-H bond in the $-NH_2$ group (for the N-H··N and N-H···π interaction) was carried out at the DFT-B3LYP/6-311++G**. Initially, it was performed for the isolated molecule in the crystal geometry of **E1**. Then, the modes of vibration for the molecular pair interacting *via* N-H··N and N-H···π interactions in **E1** have been carried out. Finally, we have taken one molecule in the crystal geometry (**E1**) where a N-H hydrogen is interacting with one phenyl ring (benzene) and the other hydrogen is interacting with the N atom of N-methylenemethanamine *via* N-H···π and N-H···N interactions respectively. The difference Fourier maps (F_{obs}-F_{cal}) in the molecular plane have been calculated by MoPro (version 15.02) software [39].

Hirsfeld surface analysis

The Hirshfeld surface associated fingerprint plots were performed using CrystalExplorer 3.1[40]. This method suggests a facile way of obtaining information on trends in crystal packing. The derivation of the Hirshfeld surface and breakdown of the corresponding 2D fingerprint-plot [41] provide a convenient means of quantifying the interactions within the crystal structures to identify the similarities and dissimilarities between related crystal structures and polymorphs.

RESULT AND DISCUSSION

The morphologies of the three different forms are shown in **Figure 1**. The bulk powder was sparingly soluble in hexane. On warming, it was observed to be completely soluble. Crystals of **E1** (more stable) were obtained on fast evaporation from hexane and the crystals of **E2** (2nd form) were obtained by slow evaporation from hexane. **E1** and **E2** correspond to the *E*-isomer of the compound. When the compound was crystallized from dichloromethane and hexane (layering method, 3:1 ratio) at low temperature (5ºC), concomitant crystals of **Z** (*Z*-

isomer) and **E2** were formed. On increasing the concentration of the polar solvent (4:1 ratio of dichloromethane and hexane at 5ºC, only the ***Z***-isomer was obtained.

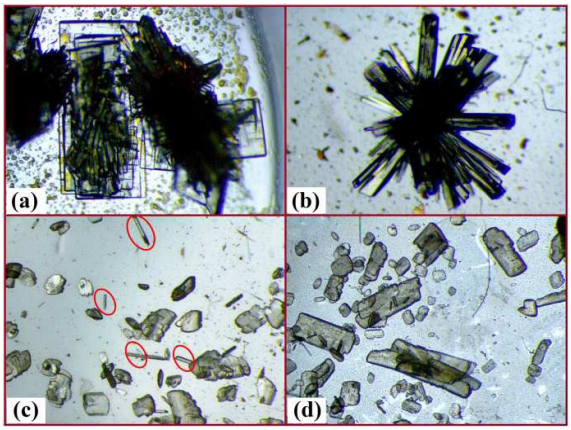

Figure 1: Microscopic images of crystals: (a) **E1**, (b) **E2**, (c) concomitant of **E2** and **Z** and (d) only **Z** isomer

Solid state conformation

ORTEP's of these isomers have been shown in **Figure 2**. It is of interest to focus on the molecular conformation around the C=N bond of 2-fluoro-*N*′-(3-fluorophenyl) benzimidamide. It consists of two phenyl rings: the first ring (containing one fluorine atom in *ortho* position) is connected with the sp^2 hybridized carbon atom C13 (attached with $–NH_2$ group) of the C=N double bond and the second ring (containing one fluorine atom in *meta* position) is connected with the nitrogen atom N1 either in same side or in opposite side (*syn* or *anti*) of the C=N bond. **E1** and **E2** adopt *E* conformation and the third form is a *Z*-isomer (**Z**). All molecules have ten proton donors and three acceptors that can take part in the hydrogen bonding (strong or weak) interactions. The C13-N1 bond distances are 1.292(2) Å, 1.296(3) Å and 1.298(2) Å for **E1**, **E2** and **Z** respectively and hence exhibits double bond formation for the C-N bond [42]. Similarly, the bond distance values [1.353 (2) Å, 1.342 (2) Å and 1.349(2) Å] for C13-N2 indicate the presence of single bond only.

Figure 3 is represented as an overlay diagram drawn between these conformers taking at the crystal geometries. List of some selected torsion angles are shown in **Table 2**. The two polymorphs (**E1** and **E2**) exhibits conformational polymorphism and the difference in torsion C1A-C13-N1-C7A is 3.4(2) º which is clearly visible in the overlay diagram (**Figure 3**) of the three isomers. After geometrical optimization (in gaseous state) performed with DFT method using B3LYP /6-31G**, **E1** and **E2** have achieved the same molecular conformation, the torsion being 9.7º. In case of **Z**, the torsion C1A-C13-N1-C7A is -175.2(1) º. The

difference in the overall geometry is mostly caused by the rotation of the ring (C7A-C8A-C9A-C10A-C11A-C12A) around the C(13) = N(1) bond.

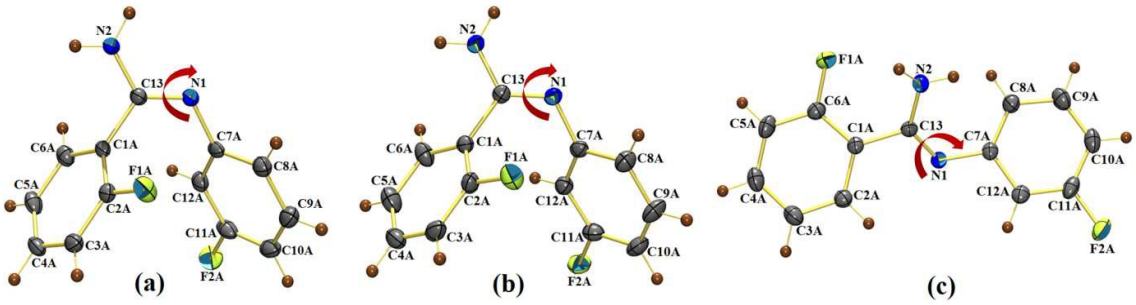

Figure 2: ***ORTEP*** view of the molecular structure of (a) **E1**, (b) **E2**, and (c) **Z**. Thermal ellipsoids are drawn at 50% probability. Bending arrows are showing the torsion angle in the asymmetric unit.

Table 2: Selected torsion angles (°) present in the molecule.

Torsion	E1	E2	Z
C2A-C1A-C13-N2	-115.9(2) *-131.4*[a]	-121.5(2) *-131.4*[a]	-135.2(1) *172.6*[a]
C1A-C13-N1-C7A	5.4(2) *9.7*[a]	8.8(3) *9.7*[a]	-175.2(1) *177.2*[a]
C13-N1-C7A-C8A	-127.8(2) *132.6*[a]	-131.0(2) *132.6*[a]	-50.1(2) *-60.2*[a]

[a] Italicised values obtained from theoretical B3LYP/6-31G** calculations

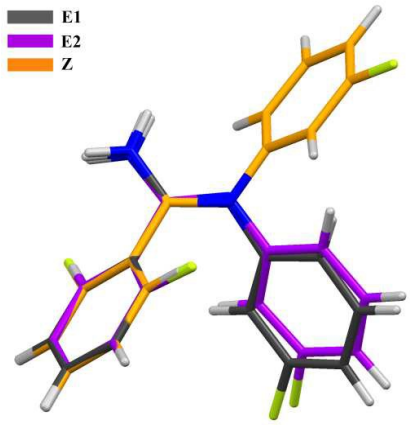

Figure 3: An overlay diagram of the conformers found in the polymorphs (**E1** and **E2**) and **Z** isomer shown with different colour code.

The complete conformational analysis was performed in order to know the relative stabilities between the *E*/*Z* isomers. Single point energy calculations were performed starting from the optimized geometry for the *E* isomer having the torsion (τ) 9.7° (with DFT-B3LYP/6-

31G**). The results show that the *E* isomer is more stable than the *Z* isomer by 22.7 kJ/mole. We have started from the optimized geometry of the *E* isomer having the torsion (τ) 9.7º. From there the (relative value is 0º) torsion (τ) has been changed through the rotation around the C=N bond by 5º. In each step, the single point energy was calculated. Finally, to 360º, the relative energies (ΔE) have been plotted with torsion angle (τ) and it gives two maxima points and two minima points (**Figure 4**). *E* isomer can be converted to the *Z* isomer through two different pathways. As the activation energy barrier for path II is much higher than the path I, the system will follow the isomerization process involving path I. The energy difference obtained from the plot (rotation along the C13-N1 bond from *Z* to *E*) is 21.8 kJ/mol, is well supported by the single point energy (at optimized geometry) difference of 22.7 kJ/mol.

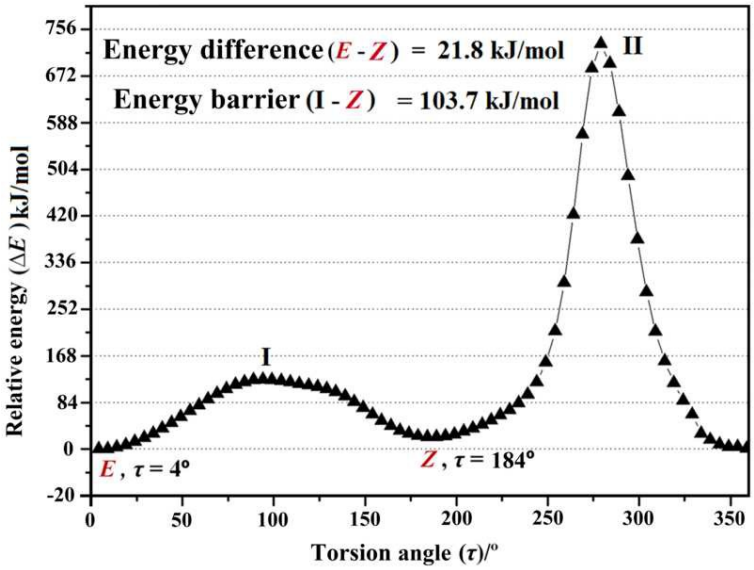

Figure 4: Plot of relative energy (ΔE) vs torsion angle (τ) due to the rotation along the C=N double bond.

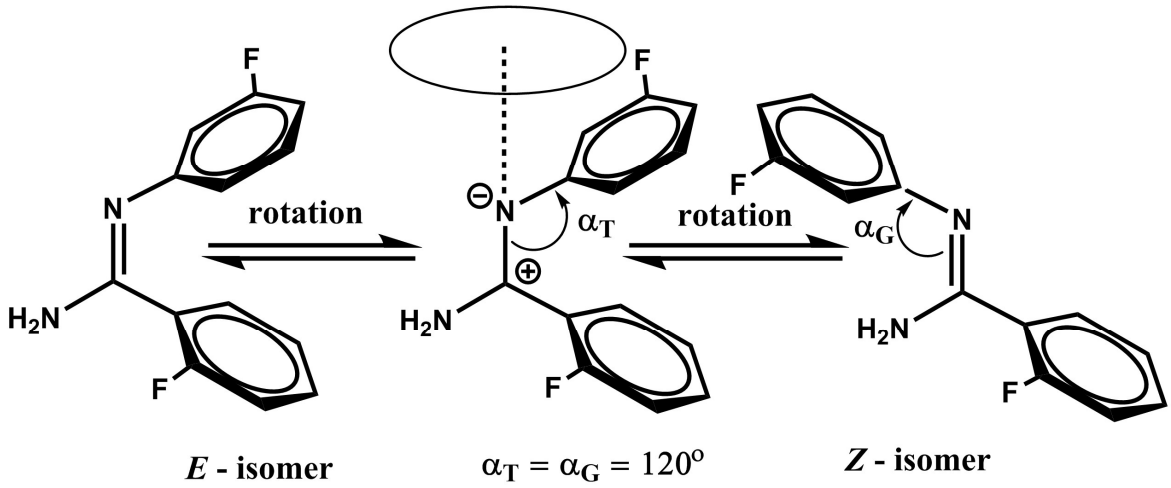

Scheme 2. Possible pathway of *E*/*Z* isomerization by rotation. α_T and α_G are the C-N-C angles at transition state and ground state respectively.

Due to the greater electronegativity of N atom than C atom, it has been assumed that the charge separation decreases the double bond character of C-N bond at the time of isomerization. In the transition state, the molecule may be considered as a dipolar species (**Scheme 2**). For this, for the *E*-isomer, the overlap between the carbon *p* orbital and sp^2 hybridized orbital for the nitrogen atom is decreased in the transition state and simultaneously the energy is increased. This leads to greater flexibility around the C-N double bond and hence the *meta*-fluorophenyl ring rotates. Finally, it adopts the *Z*-isomeric configuration leading to greater overlap in the final product. It is to be noted that the transition state wherein the charge on the carbocation may be stabilized by electron donation from the $-NH_2$ group.

The thermal stabilities of these isomers were evaluated using differential scanning calorimetry (DSC of bulk, crystals of **E1**, **E2** and **Z**) and hot stage microscopy (HSM) methods. On heating of the bulk powder, only one endothermic peak at 80.3ºC was observed s**Figure 5**). There was no solidification (exothermic) peak during cooling process at same cooling rate (3ºC/min). **E1** (having unique sharp endothermic peak), the more stable form, melts at higher temperature (89.7 ºC) compared to the bulk powder. The **E2** form has DSC traces similar with that of the bulk one. **Z** crystals show change in crystal characteristics before melting. On heating of **Z** crystals, two endothermic peaks were observed. The first one at 66.4ºC represents the existence of a possible phase transformation of **Z** isomer to the configurational **E2** isomer followed by melting at 81.2ºC (the second endothermic peak, same temperature as the bulk compound).

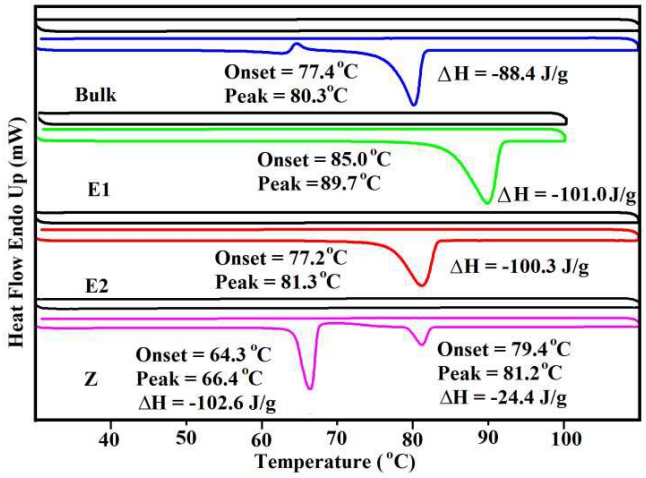

Figure 5: DSC heating/cooling curves of the polymorphs (**E1** and **E2**) and **Z** isomer recorded at a heating rate of 3ºC/min.

To investigate the nature of phase transformations, hot stage microscopy (HSM) measurements on the single crystals were carried out. Crystals of **E1** and **E2** (two polymorphic forms of *E*-isomer) were taken together on a glass slide and heated from 25ºC to 90ºC (the heating rate 0.5ºC/min) inside the hot stage apparatus (**Figure S2**). We have observed that the **E2** form first started melting at 77.5ºC and melted completely at 81ºC. During this heating period, the **E1** form does not exhibit any changes. **E1** form started melting at 85ºC and was completely melted at 89.4ºC. Again we have performed the experiment taking the crystals of **E2** and **Z** together with the same heating rate of 0.5ºC/min (**Figure 6** and **Figure S3**). During heating, at 60ºC small needles were visible inside the crystal of **Z**. This change was clearly visible under the microscope, but appeared as dark lines in the images taken. At 64ºC the **Z** crystal was fully converted to a new form which consisted of dark lines (small needles). No changes were observed in the **E2** form. At 77.5ºC, both the forms started undergoing a physical transformation together and melted completely at 81ºC. Furthermore, after 3-4 hours during the second heating process (re-heating) both the solids melted together at 80.5ºC. So, the results observed from the DSC and HSM measurements support the fact that during the heating cycle, the phase transition corresponds to the *Z*/*E* isomerization.

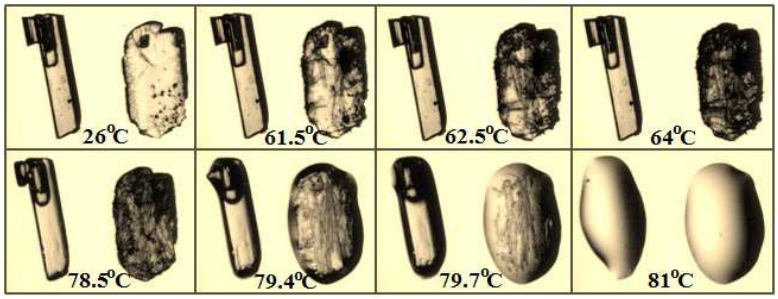

Figure 6: Hot-stage microscopy snapshots of *E*/*Z* isomers (**E2** and **Z**) at different temperatures on heating @ 0.5ºC/min.

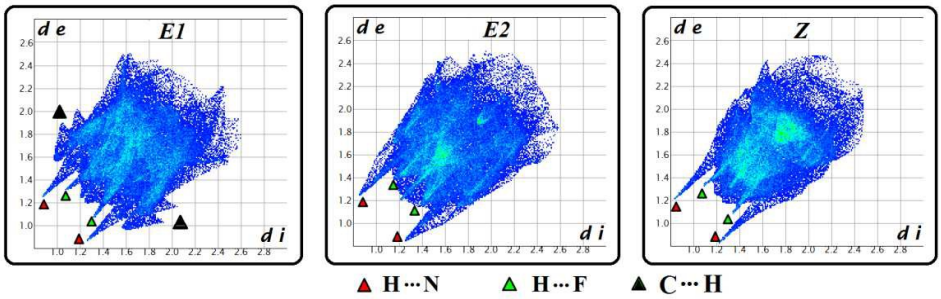

Figure 7: Hirshfeld surface fingerprint plots of the two polymorphs (**E1** and **E2**) and **Z**-isomer. The spikes labelled with red (H···N interactions), green (H···F interactions) and black (C···H interactions) triangles depicts the characteristic features of the fingerprint plots.

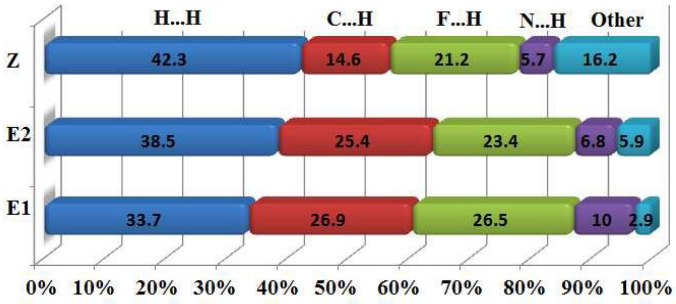

Figure 8: Relative contribution of various atom···atom contacts contributing towards the crystal packing of the different isomers.

It is noteworthy that each form has a unique molecular arrangement. **Figure 7** shows the differences in the fingerprint plots of the three forms. The spikes were labelled with various colour which are the significant contributions coming from different intermolecular contacts existing in the crystal. The sharp spikes represent their importance in the formation of a given

crystal structure. The contribution associated with the C···H (26.9%), F···H (26.5%) and N···H (10.0%) intermolecular contacts for **E1** form is higher than the other two forms (**E2** and **Z**, **Figure 8** and **Figure S7**).

Table 3: Interaction energy (in kJ/mol) of the molecular pairs and related intermolecular interaction with their geometry.

Motifs	Symmetry code	Centroid-centroid distance (Å)	E_{Coul}	E_{Pol}	E_{Disp}	E_{Rep}	E_{Tot} / E^a	Possible involved Interactions	Geometry (Å/ °)
					E1				
I	-x+2, y+1/2, -z+3/2	7.483	-34.9	-18.9	-30.7	41.6	-42.8/-42.8	N2-H2B...N1 N2-H2A...Cg1	2.13, 148 2.39, 160
II	x, -y+1/2, z+1/2	6.255	-8.8	-4.6	-27.7	19.7	-21.4/-20.6	C3A-H3A...F2A C5A-H5A...N1	2.40, 137 2.60, 157
III	-x+1, -y, -z+1	6.683	-4.2	-2.5	-26.9	14.3	-19.3/-21.0	C10A-H10A...F1A C9A-H9A...F1A C9A...C9A	2.63, 121 2.70, 119 3.591(2)
IV	x, y+1, z	8.377	-5.5	-2.9	-17.6	13.9	-12.2/-15.9	C4A-H4A...Cg2	2.67, 133
V	-x+1, y-1/2, -z+1/2	7.738	-2.5	-1.7	-13.4	5.5	-12.2/-13.9	C3A-H3A...F2A C10A-H10A... π (C4A)	2.40, 137 2.99, 141
VI	-x+2, -y+1, -z+1	9.094	1.3	-1.3	-13.4	7.2	-6.3/-7.6	C5A...C6A	3.638(2)
VII	x, -y-1/2, z+1/2	8.310	0.0	-0.8	-8.0	3.4	-5.5/-6.3	C9A-H9A...F2A C8A-H8A...F2A	2.85, 117 2.67, 111
					E2				
I	-x+1, -y, -z+2	8.009	-36.6	-12.2	-19.3	22.6	-45.4/-45.0	N2-H2A...N1	2.34, 148
II	x, -y, z-1/2	6.771	-28.9	-14.1	-35.8	39.5	-39.5/-41.2	N2-H2B...N1 C6A-H6A...C5A	2.09, 152 2.98, 147
III	x, -y+1, z-1/2	7.558	-4.0	-2.2	-16.6	9.5	-13.3/-14.7	C9A-H9A...F1A	2.66, 134
IV	x, y, z-1	8.124	-4.6	-2.1	-15.1	9.7	-12.2/-16.4	C4A-H4A...F2A C3A-H3A... π (C10A)	2.59, 128 2.93, 145
V	-x+1/2, y-1/2, -z+3/2	8.366	-4.6	-1.3	-8.4	4.2	-10.1/11.3	C6A-H6A...F2A C5A-H5A...F2A	2.68, 122 2.64, 123
VI	-x+1/2, -y+1/2, -z+2	7.502	-0.8	-1.3	-8.0	3.8	-6.7/-8.8	C12A-H12A...F2A	2.66, 130
VII	-x+1, y, -z+3/2	5.893	-5.0	-2.9	-26.2	17.8	-6.4/-7.2	C8A-H8A...F1A F1A...F1A N2...N2	2.57, 127 2.711(2) 3.178(2)
					Z				
I	x+1/2, -y+1/2, z-1/2	5.041	-37.4	-17.2	-43.7	55.0	-43.3/-45.8	Cg1...Cg2 N2-H2D...N1	3.701(2) 2.04, 150
II	x+1/2, -y+1/2, z+1/2	4.920	-4.6	-2.9	-34.0	20.2	-21.5/-31.7	Cg1...Cg2 N2...F1A	4.182(2) 2.984(2)
III	x-1, y, z	6.782	-4.6	-2.5	-20.2	10.9	-16.4/-16.8	C2A-H2A...F1A C8A-H8A...F2A	2.44, 148 2.53, 119
IV	-x+1/2, y-1/2, -z+1/2	12.016	-3.4	-1.3	-9.3	5.0	-9.0/-7.6	C10A-H10A...F2A	2.59, 135
V	-x, -y+1, -z+1	10.546	-2.5	-0.8	-10.1	5.0	-8.4/-10.5	π...π	3.715(2)

E^a is the stabilization energy performed using DFT-Disp/B97D using aug-cc-pVTZ.

Table 4: Lattice energy (in kJ/mole) of the three isomers.

Code	E_{Coul}	E_{Pol}	E_{Disp}	E_{Rep}	E_{Tot}
E1	-60.5	-29.4	-128.5	95.3	-123.9
E2	-61.3	-26.1	-127.7	93.2	-121.8

Z	**-56.3**	**-26.9**	**-132.3**	**99.9**	**-115.5**

The single crystal X-ray diffraction revealed that **E1** crystallizes in the space group $P2_1/c$ with $Z = 4$. The crystallographic parameters are shown in **Table 1**. The molecules in the crystal lattice adopt a herringbone packing arrangement [43] down the *bc* plane associated with strong N-H···N hydrogen bonds along with N-H···π and C-H···π intermolecular interactions (**Figure 9**). In the crystal, the strongest interaction was formed *via* the adjacent 2_1 screw related molecules which are connected together with N-H···N hydrogen bond (involving H2B with N1) and N-H···π (involving H2A with Cg1) intermolecular interaction. The corresponding interaction energy is -42.8/-42.8 kJ/mol (obtained from PIXEL and DFT +Disp method) wherein the Coulombic contribution (41%) is more significant than the polarization (21%) and dispersion (36%) contributions. In the herringbone arrangement, along the *b* axis the adjacent molecules (having similar orientations) were connected with C-H···π (involving H4A with Cg2) interaction lead to formation a zig-zag chain and the corresponding interaction energy is -12.2/-15.9 kJ/mol.

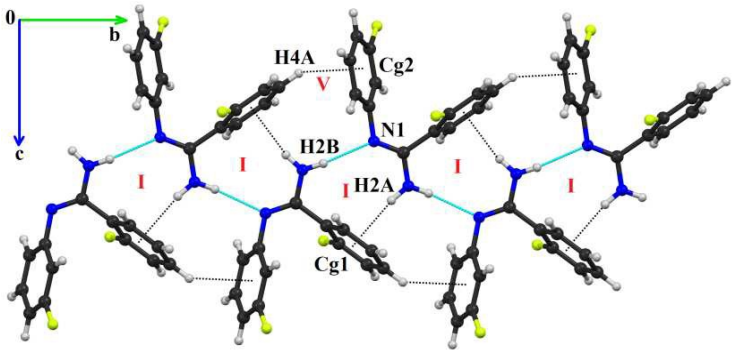

Figure 9: Packing network of **E1** showing the herringbone packing arrangement of molecules connected with N-H···N chain associated with N-H···π and C-H···π down the *bc* plane.

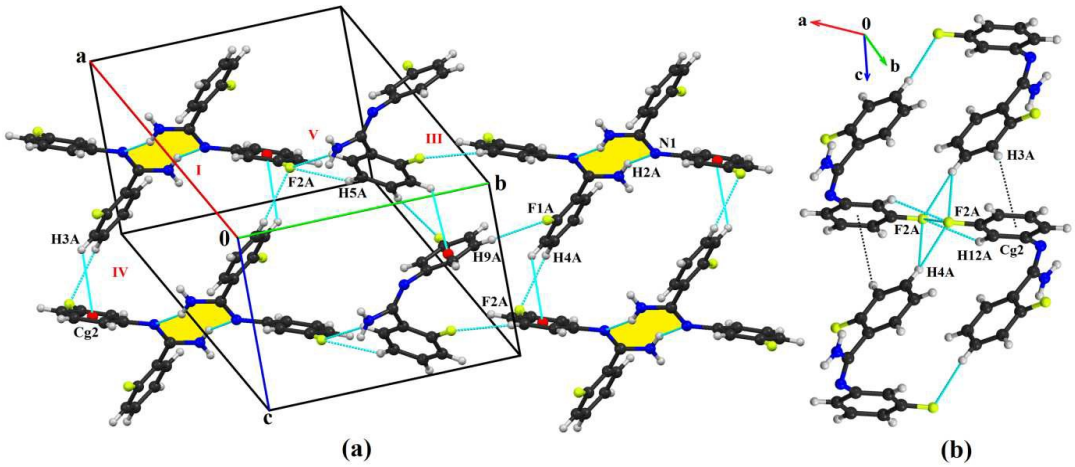

Figure 10: (a) Assembly of **E2** molecules having centrosymmetric N-H···N synthon associated with weak C-H···F intermolecular interactions down the *ab* plane, (b) showing the bifurcated C-H···F interaction and F···F contact.

E2 crystallizes in the monoclinic centrosymmetric *C*2/*c* space group with one molecule in the asymmetric unit. In the crystal, the molecules were found to form a centrosymmetric supramolecular synthon $\mathbf{R_2^2(8)}$ *via* N-H···N strong hydrogen bond (H···N distance = 2.34 Å) involving N1 with H2A (**Figure 10**). The corresponding stabilization energy of this dimer is around **-**45.4/-45.0 kJ/mol wherein the Coulombic contribution (53%) is more significant than the polarization (17%) and dispersion (28%) contributions. These molecular dimers behave as a single unit form an alternate layer along the *a*-axis and are connected with C-H···F (involving F1A with H9A) and C-H···π (involving C10A with H3A) intermolecular interactions. Another hydrogen atom (H2B) of the $–NH_2$ group was also involved in the formation of a strong N-H···N hydrogen bond interacting (H···N distance = 2.09 Å) with N1 atom and the stabilization energy is -39.5/-41.2kJ/mol. **Z** form crystallizes in a centrosymmetric $P2_1/n$ space group with Z′ = 1. Crystal structure analysis reveals that the molecules were found to form an N-H···N molecular chain down the (101) plane associated with π-π stacking (**Figure 11**). The strongest molecular pair (**I**) was formed *via* strong N-H···N hydrogen bond having short H···N distance 2.04Å and the angularity was 150º. The corresponding stabilization energy is -43.3/-45.8 kJ/mol. The molecules form a planar sheet through the involvement of weak C-H···F intermolecular interactions (**III** and **IV**) down the *ab* plane. The sheet contains centrosymmetric C-H···F interactions having the pairing energy -9.0/-7.6 kJ/mol (which molecular pairs). The molecular pairs and their stabilization energies were shown in **Figure S4-S6**. **Table 3** lists the total lattice energy of the individual

compounds in the range of −115 to −124 kJ/mol where the dispersion has the major contribution (56%) toward the total lattice energy rather than the Coulombic (27%) and polarization (13%) contribution.

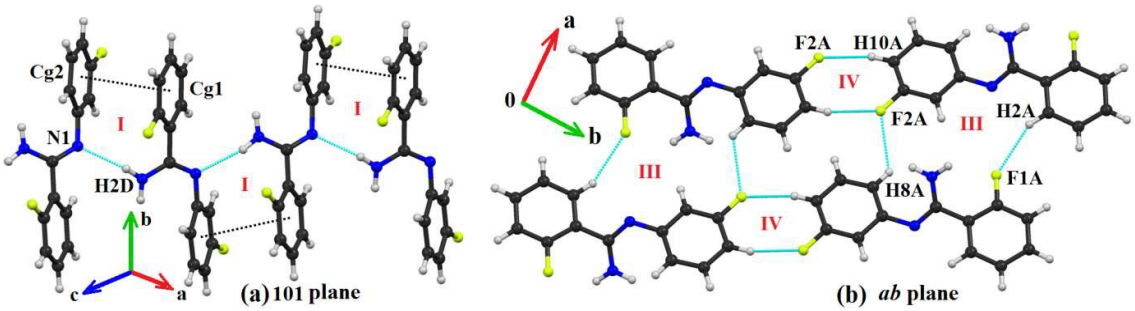

Figure 11: Crystal packing view of **Z** (a) down the 101 plane showing molecular chain *via* strong N-H···N hydrogen bond associated with π···π stacking (b) down the *ab* plane showing the layer of $\mathbf{R^2_2(8)}$ synthon *via* C-H···F interactions.

From the crystal packing features of the two polymorphs (*E*-isomers) and *Z*-isomer, the main difference is that both the hydrogen atoms (H2A and H2B) connected with N2 atom were involved in the formation of a strong N-H···N hydrogen bond in **E2**. But in case of **E1**, only one hydrogen atom (H2B) is engaged in N-H···N formation and the other one (H2A) interacts *via* N-H···π interaction with centroid Cg1. Whereas in **Z**, the H2C atom of the $-NH_2$ group is not involved in any interaction but the hydrogen atom H2D forms N-H···N hydrogen bond. We have observed the differences in the packing arrangement of the molecules. Each form has a unique molecular arrangement. In case of **E,** the adjacent molecule arranged in such a way that, when one hydrogen of $-NH_2$ group is involved in N-H···N hydrogen bonding, there exists no possibility for the formation of another N-H···N hydrogen bond. As, those two adjacent molecules are related by a 2_1 screw axis. So, there was only one possibility, to form N-H···π interaction with the phenyl ring (Cg1) of the other molecule. In **Figure 9**, the orientation of the phenyl rings on adjacent molecules adopt a perpendicular orientation. $\mathbf{R_2^2}$ **(8)** motif formed via weak C-H···F interaction is unique in case of **Z**, which was not present in **E1**. In solution at low temperature (< 5ºC) during nucleation of the **E2** isomer (bulk powder), the phenyl ring (Cg2) rotates around the C=N bond to attain the **Z** isomer. When the *E*-isomer was converted to *Z*-isomer, then π···π stacking was formed instead of N-H···π interaction (observed in **E1**) or N-H···N homo-synthon (observed in **E2**).

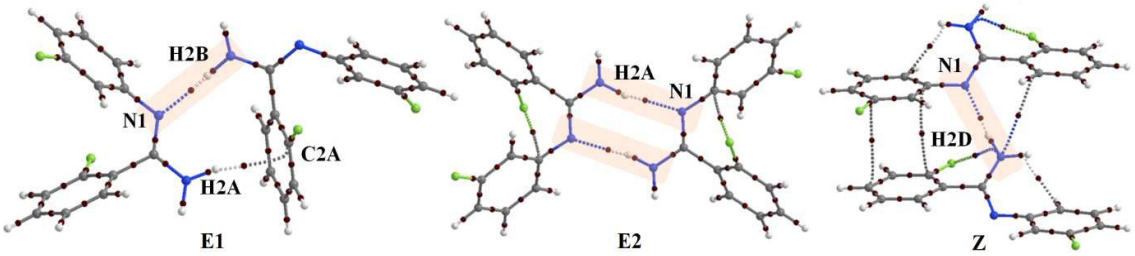

Figure 12: Molecular graphs depicting the bond critical points between the N-H proton (H2A) and ring carbon (C2A) in **E1**.The N-H···N interactions indicate the bond critical points in red bold circle in **E1**, **E2** and **Z**.

In order to evaluate the topological characteristics of the N-H···π interaction, we have performed a topological analysis using the method of QTAIM [44]. It is of interest to evaluate whether it can be deemed to be a "hydrogen bond" in accordance with the rules of IUPAC [45]. The values of the electron density [ρ(r) = 0.064 e/Å^3], the Laplacian [$\nabla^2\rho$(r) = 0.740 e/Å^5] of the electron density and the local kinetic energy density (E_{int} = 7.0 kJ/mol) at the bond critical point (BCP) and the shape of the bond path linking the N-H hydrogen (H2A) with the ring carbon (C2A) confirm the existence of the N-H···π interaction (**Figure 12** and **Table 5**).

Table 5: Topological parameters at the bond critical point (BCP's) of selected intermolecular interactions.

Code	Interaction	d(Å)	R_{ij}(Å)	ρ_{BCP} (e/Å^3)	$\nabla^2\rho_{BCP}$ (e/Å^5)	V_b (a.u.)	G_b (a.u.)	D.E^V/D.E^G (kJ/mol)
E1	N2-H2B···N1	2.13	2.15	0.142	1.585	-0.013619	0.015029	17.9/17.0
	N2-H2A···π (C2A)	2.54	3.05	0.064	0.740	-0.004739	0.006207	6.3/7.0
E2	N2-H2A···N1	2.34	2.37	0.094	0.967	-0.007655	0.008842	10.1/10.0
Z	N2-H2D···N1	2.04	2.07	0.167	1.869	-0.017354	0.018370	22.9/20.8
	N2···F1A (intra)	2.84	2.99	0.081	1.253	-0.009982	0.011489	13.2/13.0

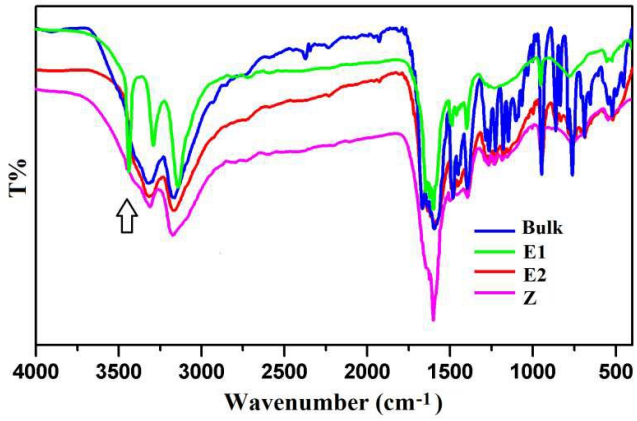

Figure 13: Infrared spectra of the three forms including bulk powder showing the significance of N-H···π interaction.

The presence of N-H···π interaction is well supported by the theoretical analysis and the vibrational spectra obtained in the solid state. In infrared spectrum of **E1** (**Figure 13**), the appearance of one new peak (of relatively high intensity, denoted by arrow) was observed at 3434 cm^{-1}, including the peaks at 3287 and 3138 cm^{-1}. This enhancement of vibrational frequency (improper spectral blue shift [46]) indicates that there is a significant H-bond interaction between the N-H group and the aromatic ring. The vibrational frequency analysis (**Figure S8-S10**) performed at the DFT-B3LYP/6-311++G** level using model dimers, also provides theoretical evidence for the existence of the new peak at 3434 cm^{-1}, attributed to the interaction of the N-H group. Profile fitting of the powder pattern has shown for the two polymorphic forms **E1** and **E2** with the bulk in **Figure 13** having Rp and Rwp values 3.20 and 4.98 respectively.

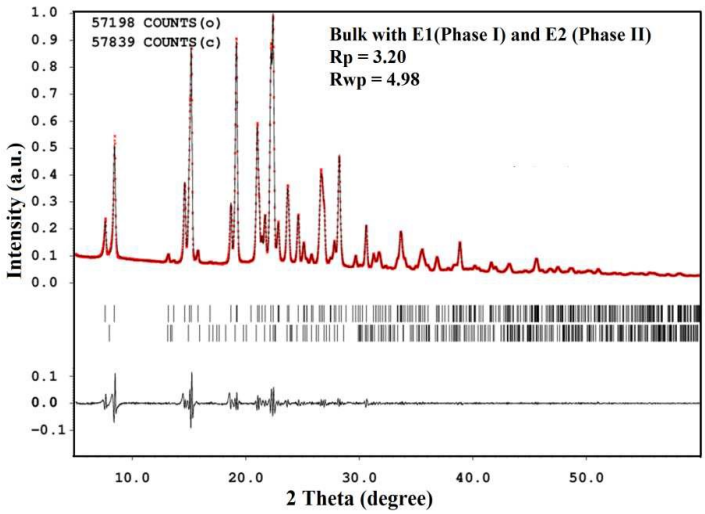

Figure 14: Profile fitting powder pattern between **E1** and **E2** with bulk.

CONCLUSIONS

Thus slow evaporation from hexane allows for the formation of pre-nucleation aggregates consisting of N-H···N dimers in **E2** whereas in case of **E1**, fast evaporation results in a combination of N-H···N and N-H···π interactions forming dimeric motifs responsible for further aggregation. In both **E1** and **E2** the molecules are involved in the maximization of the hydrogen bonding capacity. On the contrary in case of **Z** this is not realised and hence it crystallizes as a low temperature form. On heating, it undergoes conversion into the high temperature form, namely **E2**. Thus intramolecular bonding enables the rotational energy barrier to be overcome and intermolecular bonding features resulting in configurational isomerism (*Z* to *E*). Thus the role of sterics though significant in the *E* isomers is compensated by stabilization *via* H-bonding interactions in the solid state. In conclusions, a molecular has been synthesized which is sensitive to the temperature of crystallization. In addition the rate of evaporation also plays a significant role in polymorph formation. This is expected to have commercial implications in the crystallization of different API's of interest in the pharmaceutical industry.

ACKNOWLEDGEMENTS

D.D. thanks IISER Bhopal for research fellowship. D.C. and D.D. thank IISER Bhopal for research facilities and infrastructure and DST-SERB for research funding.

REFERENCES

1. J. Bernstein, *Polymorphism in Molecular Crystal*s. Oxford University Press; New York. 2002.

2. (a) J. Bernstein, *Organic Solid State Chemistry*, Elsevier; Amsterdam, 1987, Ch. 13; (b) S. R. Byrn, *Solid-State Chemistry of Drugs*, Academic Press; New York, 1982, Ch. 4.

3. (a) K. E. Riley, M. Pitonak, P. Jurecka, P. Hobza, *Chem. Rev.*, 2010, **110**, 5023; (b) K. Müller-Dethlefs, P. Hobza, *Chem. Rev.*, 2000, **100**, 143; (c) D. Dey, T. P. Mohan, B. Vishalakshi and D. Chopra, *Cryst. Growth Des.*, **2014**, *14*, 5881.

4. (a) G. R. Desiraju, *J. Am. Chem. Soc.*, 2013, **135**, 9952; (b) G. R. Desiraju, *Cryst. Growth Des.*, 2011, **11**, 896; (c) M. Simard, D. Su and J. D. Wuest, *J. Am. Chem. Soc*., 1991, **113**, 4696.

5. (a) J. W. Chung, S. –J. Yoon, B. –K. An, and S. Y. Park, *J. Phys. Chem. C,* 2013, **117**, 11285; (b) J. Wang, J. Mei, R. Hu, J. Z. Sun, A. Qin, and B. Z. Tang, *J. Am. Chem. Soc.*, 2012, **134**, 9956; (c) S. M. Landge and I. Aprahamian *J. Am. Chem. Soc*., 2009, **131**, 18269; (d) E. H. P. Tan, G. C. Lloyd-Jones, J. N. Harvey, A. J. J. Lennox, and B. M. Mills, *Angew. Chem. Int. Ed*., 2011, **50**, 9602; (e) S. –L. Zheng, M. Messerschmidt and P. Coppens, *Acta Crystallogr.,* 2007, **B63**, 644.

6. K. Jakusova, J. Donovalova, M. Gaplovsky, M. Cigan, H. Stankovicova and A. Gaplovsky *J. Phys. Org. Chem.*, 2013, **26** 805.

7. J. Galvez and A. Guirado, *J. Comput. Chem.*, 2010, **31**, 520.

8. L. Greb and J. –M. Lehn, *J. Am. Chem. Soc.*, 2014, **136**, 13114.

9. J. H. Matthews, L. C. Paul and D. Y. Curtin *J. Chem. Soc.*, *Perkin Trans. 2*, 1991, 113.

10. (a) O. Attanasi, S. Bartoccini, G. Giorgi, F. Mantellini, F. R. Perrulli, and S. Santeusanio, *Tetrahedron*, 2010, **66**, 5121; (b) S. V. Bhosale, U. D. Patil, M. B. Kalyankar, S. V. Nalage, V. S. Patil, and K. R. Desale, *J. Heterocycl. Chem.*, 2010, **47**, 691; (c) X. Deng, and N. S. Mani, *Eur. J. Org. Chem.*, 2010, 680; (d) Y. Ohta, Y. Tokimizu, S. Oishi, N. Fuji, and H. Ohno, *Org. Lett.*, 2010, **12**, 3963; (e) Y. Wang, H. Wang, J. Peng, and Q. Zhu, *Org. Lett.*, 2011, **13**, 4604; (f) Y. –J. Zhang, D. Wang, H. –L. Zhang and Y. -G. Wang, *Acta Crystallogr.,* 2012. **E68**, o726.

11. A. Y. Volkonskii, E. M. Kagramanova, N. D. Kagramanov, and N. D. Chkanikov, *Russ. Chem. Bull., Int. Ed.*, 2012, **61**, 2001.

12. W. Szczepankiewicz, J. Suwinski and Z. Karczmarzyk, *Chem. Heterocycl. Compd.*, (N. Y.) 2004, **40**, 801.

13. A. Schmidpeter, R. K. Bansal, K. Karaghiosoff, F. Steinmüller and C. Spindler, *Phosphorus, Sulfur Silicon Relat. Elem.*, 1990, **49/50**, 349.

14. L. Capuano, W. Fischer, H. Scheidt and M. Schneider, *Chem. Ber.*, 1978, **111**, 2497.

15. Y. G. Shermolovich, V. S. Talanov, V. V. Pirozhenko and L. N. Markovskii, *Russ. J. Org. Chem.*, 1982, **18**, 2240.

16. (a) T. Asano, T. Yoshikawa, H. Nakamura, Y. Uehara and Y. Yamamoto, *Bioorg. Med. Chem.Lett.*, 2004, **14**, 2299; (b) T. Asano, T. Yoshikawa, T. Usui, H. Yamamoto, Y. Yamamoto, Y. Uehara and H. Nakamura, *Bioorg. Med.Chem.*, 2004, **12**, 3529; (c) H. Nakamura, Y. Sasaki, M. Uno, T. Yoshikawa, T. Asano, H. S. Ban, H. Fu- kazawa, M. Shibuya and Y. Uehara, *Bioorg. Med.Chem.Lett.*, 2006, **16**, 5127.

17. P. A. Koutentis and S. I. Mirallai, *Tetrahedron*, 2010, **66**, 5134.

18. (a) B. E. Smart, *J. Fluorine Chem.* 2001, **109**, 3; (b) H. Roesky, *Nat. Chem.* 2010, **2**, 240; (c) R. K. Filler, *Biomedical Effects of Fluorine Chemistry*, Kodama Ltd, Elsevier, Tokyo, Amsterdam, 1982. (d) Hiyama, T. *Organofluorine Compounds, Chemistry and Applications*, Springer, Berlin, 2000.

19. P. Panini, and D. Chopra, *Cryst. Growth Des.* 2014, **14**, 3155.

20. G. R. Desiraju and T. Steiner, *The Weak Hydrogen Bond*: *In Structural Chemistry and Biology*, Oxford University Press. The University of Michigan, 1999.

21. M. Oki and H. Iwamura, *Bull. Chem. Soc. Jpn.* 1959, **32**, 955.

22. (a) M. Nishio and M. Hirota, *Tetrahedron*, 1989, **45**, 7201; (b) M. Nishio, *Phys. Chem. Chem. Phys.* 2011, **13**,13873.

23. S. Tsuzuki, K. Honda, T. Uchimaru, M. Mikami and K. Tanabe, *J. Am. Chem. Soc.*, 2000, **122**, 11451.

24. (a) S. R. Mohapatra, K. Ramanathan, V. Shanthi, S. Srivastava and R. Sethumadhavan, *Int J Pharm Pharm Sci.*, 2011, **3**, 106; (b) V. Shanthi and R. Sethumadhavan, *Int J Pharm Pharm Sci.*, 2011, **3**, 138.

25. Apex2, Version 2 User Manual, M86-E01078, Bruker Analytical X-ray Systems Madison, WI, 2006.

26. Siemens, SMART System, Siemens Analytical X-ray Instruments Inc. Madison, MI, 1995.

27. A. Altomare, M. C. Burla, G. Camalli, G. Cascarano, C. Giacovazzo, A Gualiardi and G. Polidori, *J. Appl. Crystallogr.*, 1994, **27**, 435.

28. G. M. Sheldrick, *Acta Crystallogr.*, 2008, **A64**, 112.

29. L. J. Farrugia, *J. Appl. Crystallogr.*, 1999, **32**, 837.

30. Sheldrick, G. M. SADABS; Bruker AXS, Inc.: Madison, WI, 2007.

31. L. J. Farrugia, *J. Appl. Crystallogr.*, 1997, **30**, 565.

32. C. F. Macrae, I. J. Bruno, J. A. Chisholm, P. R. Edgington, P. McCabe, E. Pidcock, L. Rodriguez-Monge, R. Taylor, J. Streek and P. A. Wood, *J. Appl. Crystallogr.*, 2008, **41**, 466.

33. M. Nardelli, *J. Appl. Crystallogr.*, 1995, **28**, 659.

34. A. L. Spek, *Acta Crystallogr.*, 2009, **D65**, 148.

35. TURBOMOLE V6.3; TURBOMOLE GmbH: Karlsruhe,Germany, 2011; available from http://www.turbomole.com.

36. (a) J. D. Dunitz and A. Gavezzotti, *Cryst. Growth Des.*, 2012, **12**, 5873; (b) L. Maschio, B. Civalleri, P. Ugliengo and A. Gavezzotti, *J. Phys. Chem. A*, 2011, **115**, 11179; (c) J. D. Dunitz and A. Gavezzotti, *Chem. Soc. Rev.*, 2009, **38**, 2622; (d) J. D. Dunitz and A. Gavezzotti, *Cryst. Growth Des.*, 2005, **5**, 2180; (e) J. D. Dunitz and A. Gavezzotti, *Angew. Chem., Int. Ed.*, 2005, **44**, 1766; (f) L. Carlucci and A. Gavezzotti, *Chem. Eur. J.*, 2005, **11**, 271; (g) A. Gavezzotti, *CrystEngComm*, 2003, **5**, 429.

37. T. A. Keith, AIMALL, version 13.05.06; TK Gristmill Software, Overland Park KS, 2013; aim.tkgristmill.com.

38. I. Mata, I. Alkorta, E. Espinosa and E. Molins, *Chem. Phys. Lett.*, 2011, **507**, 185.

39. (a) C. Jelsch, B. Guillot, A. Lagoutte and C. Lecomte, *J. Appl. Cryst.* 2005, **38**, 38; (b) B. Guillot, L. Viry, R. Guillot, C. Lecomte and C. Jelsch, *J. Appl. Cryst.* 2001, **34**, 214. http://www.crystallography.fr/crm2/fr/services/logiciels/MoPro.htm

40. S. K. Wolff, D. J. Grimwood, J. J. McKinnon, M. J. Turner, D. Jayatilaka and M. A. Spackman, CrystalExplorer, version 3.0; University of Western Australia: Crawley, Australia, 2012.

41. M. A. Spackman and J. J. McKinnon, *CrystEngComm*, 2002, **4**, 378.

42. F. H. Allen, O. Kennard and D. G. Watson, *J. Chem. Soc., Perkin Trans.* 2,1987, S1.

43. V. R. Vangala, B. R. Bhogala, A. Dey, G. R. Desiraju, C. K. Broder, P. S. Smith, R. Mondal, J. A. K. Howard and C. C. Wilson, *J. Am. Chem. Soc.*, 2003, **125**, 14495.

44. (a) R. F. W. Bader, *Atoms in Molecules: A Quantum Theory*; Oxford University Press: Oxford, U.K., 1990. (49) V. G. Tsirelson, *In The Quantum Theory of Atoms in Molecules*: *From Solid State to DNA and Drug Design*; C. Matta, R. Boyd, Eds.; Wiley-VCH: Weinheim, Germany, 2007; Ch 10.

45. E. Arunan, G. R. Desiraju, R. A. Klein, J. Sadlej, S. Scheiner, I. Alkorta, D. C. Clary, R. H. Crabtree, J. J. Dannenberg, P. Hobza, H. G. Kjaergaard, A. C. Legon, B. Mennucci and D. J. Nesbitt, *Pure & Appl. Chem.*, 2011, **83**, 1619.

46. B. J. Veken, W. A. Herrebout, R. Szostak, D. N. Shchepkin, Z. Havlas and P. Hobza *J. Am. Chem. Soc.*, 2001, **123**, 12290.

TABLE OF CONTENTS (TOC):

Manuscript title: N-H···π induced configurational isomerism and the role of temperature in the *Z* to *E* isomerization of 2-fluoro-*N*′-(3-fluorophenyl) benzimidamide.

Authors: Dhananjay Dey and Deepak Chopra

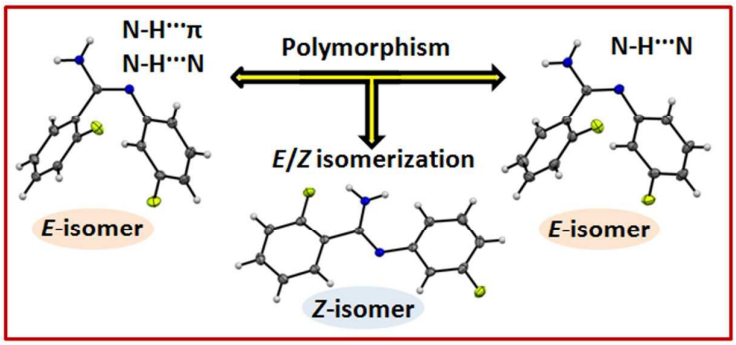

The role of temperature in polymorphism and the isolation of configurational isomers of 2-fluoro-*N*′-(3-fluorophenyl) benzimidamide have been investigated.